THE JOURNAL OF PHYSICAL CHEMISTRY C
A JOURNAL OF THE AMERICAN CHEMICAL SOCIETY

pubs.acs.org/JPCC
Article

Effect of Substrate on Sulfur Vacancy Defect-Mediated Photoluminescence in Two-Dimensional MoS_2

Yiru Zhu, Zhepeng Zhang, Ye Wang, Soumya Sarkar,* Yang Li, Han Yan, Larissa Ishibe-Veiga, Anita Bagri, Ziwei Jeffrey Yang, Hugh Ramsden, Goki Eda, Robert L.Z. Hoye, Yan Wang, and Manish Chhowalla*

Cite This: J. Phys. Chem. C 2025, 129, 8294–8302

Read Online

ACCESS | Metrics & More | Article Recommendations | Supporting Information

ABSTRACT: Chalcogen vacancy defects in monolayer transition metal dichalcogenides form in-gap states that can trap excitons, leading to defect-mediated photoluminescence (PL) emission. Here, we show that room-temperature (RT, 300 K) PL from sulfur vacancies in defective monolayer MoS_2 is sensitive to doping from dielectric substrates such as SiO_2 and HfO_2. The defect-mediated PL is observed for monolayer MoS_2 on untreated HfO_2 but is quenched on untreated SiO_2, which is attributed to electron doping of MoS_2 on SiO_2. Electron doping of MoS_2 is confirmed by Raman and synchrotron X-ray photoelectron spectroscopy. Annealing of the SiO_2 substrate modifies its surface states, which is reflected in the recovery of the defect-mediated PL emission. The role of substrate-induced doping on sulfur vacancy-mediated PL is further supported by gate-dependent PL measurements. Our results suggest that excess electrons fill the defect energy states from sulfur vacancies in MoS_2, reducing the probability of photoexcited carrier occupation and subsequent defect-mediated emission.

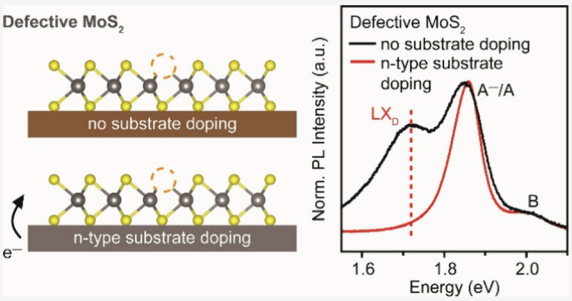

Defects in two-dimensional (2D) transition metal dichalcogenides (TMDs) have properties that are useful for optoelectronics,[1] sensing,[2] and electro/photocatalysis.[3,4] These properties are related to defect-induced in-gap states that modify the electronic structure of the host crystal. The in-gap states can trap excitons and give rise to defect-mediated photoluminescence (PL)[5,6] and even single-photon emission.[7,8] Defect-engineered TMDs, such as MoS_2 and WSe_2, have shown the ability to host quantum emitters, but their operation is currently limited to cryogenic temperatures, typically below 150 K.[8] This limitation highlights the need for further research to improve the thermal stability and performance of defect-related PL in TMDs, including defect engineering[9] and external environment (e.g., substrate) engineering. Compared with defects in 3D semiconductors, defects in 2D semiconducting TMDs are subject to reduced dielectric screening that leads to enhanced Coulombic interactions. As a result, their electronic and optical properties are susceptible to external stimuli such as strain,[10−12] dielectric screening,[13−15] and charge transfer.[16,17] These effects often originate from the dielectric substrates on which monolayer TMDs are placed. Although the effect of the substrate on the excitonic PL emission from monolayer TMDs at ∼1.9 eV is well studied,[18] how the properties of the substrate influence defect-mediated PL emission has not been well explored—partially because the methods used to introduce defects to the TMDs can also modify the underlying substrate.[19] A recent study showed that c-sapphire substrate can electron-dope MoS_2 and quench the defect PL emission at 10 K,[20] consistent with previous reports on the tunability of single-photon emission from atomic defects at 80 K through electrostatic gate control.[21] However, the effect of dielectric substrates on chalcogen vacancy defects and their PL emission at room temperature is not yet clear. Understanding these effects is critical, as they could significantly influence the performance of optoelectronic devices. For instance, in light-emitting diodes (LEDs), chalcogen vacancies can influence emission characteristics, while in photodetectors and solar cells, they can affect light absorption and charge carrier dynamics, leading to tunable emission wavelengths, enhancing light−matter interactions, and optimizing charge carrier lifetimes at localized states. Such insights would not only improve the reliability of single-photon emitters and boost photovoltaic efficiency but also enable the design of optoelectronic devices with higher performance and greater energy efficiency.

We recently reported room-temperature (RT, ∼300 K) PL from sulfur vacancies that were generated by thermally

Received: December 16, 2024
Revised: April 2, 2025
Accepted: April 3, 2025
Published: April 18, 2025

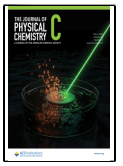

https://doi.org/10.1021/acs.jpcc.4c08491
J. Phys. Chem. C 2025, 129, 8294−8302

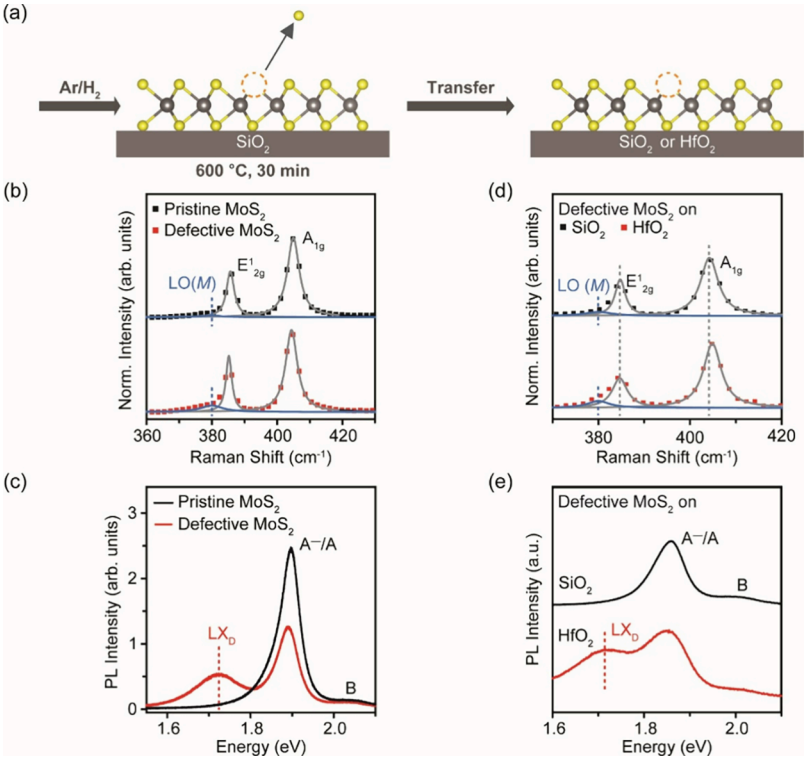

Figure 1. Transfer of defective monolayer MoS_2 (Ar/H_2 annealed) onto untreated SiO_2 and HfO_2, respectively. (a) Schematic of defective MoS_2 transferred from the original SiO_2 substrate to other substrates. (b) Raman spectra of pristine and defective MoS_2 on original SiO_2, normalized to the intensity of the Si reference peak. Pristine MoS_2 shows the characteristic E^1_{2g} in-plane mode and the A_{1g} out-of-plane mode, denoted in gray. Defective MoS_2 shows an additional LO(M) phonon mode that is taken as a signature of sulfur vacancies, denoted in blue. (c) RT PL spectra of pristine and defective MoS_2 on the original SiO_2. Pristine MoS_2 shows the A^-/A peak and the B exciton peak, while defective MoS_2 shows an additional LX_D emission that is mediated by sulfur vacancies. (d) Raman spectra of transferred defective monolayer MoS_2, normalized to the intensity of Si reference peak. The LO(M) mode remains in transferred samples, implying that the transferred samples remain defective. (e) PL spectra of transferred defective monolayer MoS_2. The LX_D peak is observed in defective MoS_2 on HfO_2, but not on SiO_2.

annealing monolayer MoS_2.[22] In this work, we investigate the influence of various dielectric substrates on sulfur-vacancy-mediated PL emission in monolayer MoS_2. This defect-mediated PL from defective MoS_2 was observed when it was placed on untreated HfO_2, but not on untreated SiO_2. This is attributed to the higher electron doping effect from SiO_2. We demonstrate modification of the surface states of dielectric substrates by annealing using synchrotron X-ray absorption spectroscopy (XAS) and water contact angle (WCA) measurements. We find that annealing SiO_2 substrates leads to reduced electron doping in MoS_2 so that defect-mediated PL can be observed. In contrast, annealing the HfO_2 substrate leads to enhanced electron doping and suppression of defect-mediated PL at room temperature in MoS_2. Our hypothesis is further supported by gate-dependent PL measurements, which show that defect-mediated PL emission is suppressed by electron doping.

RESULTS AND DISCUSSION

Monolayer MoS_2 samples on SiO_2 (300 nm)/Si wafers were prepared by mechanical exfoliation and annealed in Ar/H_2 (95 vol %/5 vol %) at 600 °C for 30 min, as shown in Figure 1a, left panel. Figure 1b shows the Raman spectrum of pristine monolayer MoS_2 with the characteristic E^1_{2g} in-plane mode at ~385 cm^{-1} and the A_{1g} out-of-plane mode at ~405 cm^{-1}. The PL spectrum in Figure 1c shows a dominant A^- (negatively charged exciton)/A (neutral exciton) PL peak at ~1.89 eV and a B exciton peak at ~2.04 eV.[23] For the annealed samples, the generation of sulfur vacancy defects was confirmed by the evolution of a satellite Raman peak [LO(M)] at ~380 cm^{-1} (Figure 1b) and PL from sulfur vacancies (LX_D) (Figure 1c)—consistent with our recent work.[22] The defective MoS_2 flake was then picked up from the SiO_2 substrate upon which it was annealed and transferred onto untreated SiO_2 and HfO_2 (thickness ~ 50 nm) substrates (Figure 1a, right panel). The untreated substrates refer to the substrates cleaned with acetone and isopropanol only without further treatment. The optimization of the transfer method is described in the Supporting Information (SI), Figures S1−S3.

The Raman spectra of transferred defective MoS_2 show the presence of the LO(M) defect mode on the two substrates (untreated SiO_2 and HfO_2), as shown in Figure 1d. The E^1_{2g} mode remains at ~385 cm^{-1} while the A_{1g} mode is hardened on HfO_2 ($\Delta\omega$ = +0.4 cm^{-1}; ω is the wavenumber of the Raman peak) than on SiO_2, indicating that MoS_2 contains a higher electron concentration ($\Delta n = +1.2 \times 10^{12}$ cm^{-2}; n is the electron concentration) on SiO_2 than on HfO_2.[24] The higher electron doping from SiO_2 than from HfO_2 is supported by synchrotron XPS measurements (SI, Figure S4). Pristine MoS_2 on SiO_2 shows the characteristic Mo 3d doublet at 230.4 eV (Mo $3d_{5/2}$), 0.54 eV higher than that of pristine MoS_2 on HfO_2, implying that MoS_2 is less electron-doped by HfO_2. The LX_D peak in PL spectra (Figure 1e) however disappears when defective MoS_2 is transferred to SiO_2 and is observed only when defective MoS_2 is transferred to HfO_2.

https://doi.org/10.1021/acs.jpcc.4c08491
J. Phys. Chem. C 2025, 129, 8294−8302

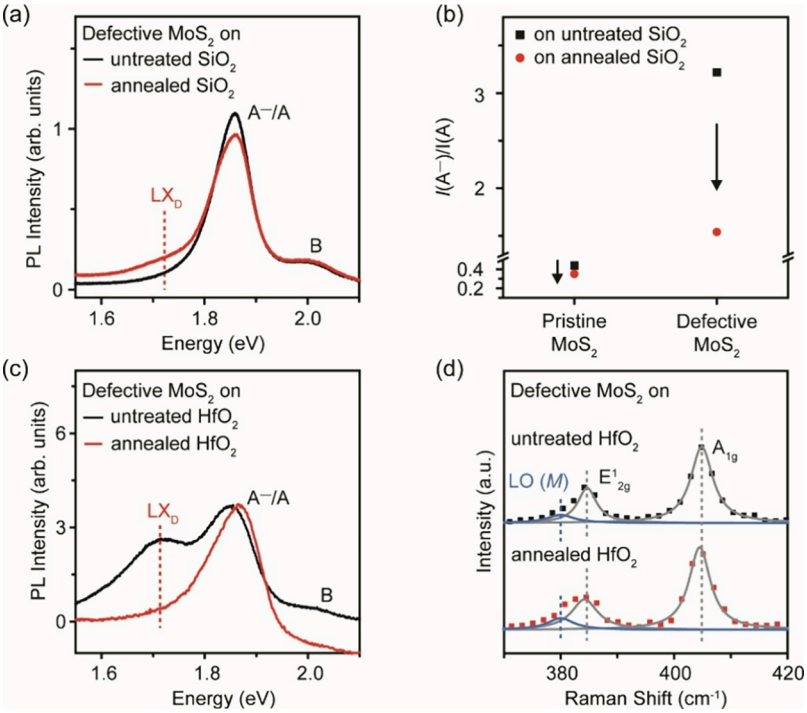

Figure 2. Transfer of defective monolayer MoS_2 onto untreated and Ar/H_2-annealed SiO_2 (600 °C, 30 min). (a) PL spectra of transferred defective monolayer MoS_2 on untreated and annealed SiO_2. The LX_D peak is observed in defective MoS_2 on annealed SiO_2 but not on untreated SiO_2. (b) Ratio of integrated intensity of the A^- trion to the A exciton, $I(A^-)/I(A)$, for pristine and defective MoS_2 on untreated and annealed SiO_2, respectively. For both pristine and defective MoS_2, the $I(A^-)/I(A)$ ratio is lower on annealed SiO_2 than that on untreated SiO_2. (c) RT PL spectra of the defective monolayer MoS_2 on HfO_2. The defective MoS_2 shows strong LX_D emission on untreated HfO_2, but not on annealed HfO_2. (d) RT Raman spectra of defective monolayer MoS_2 on HfO_2. The red shift of the A_{1g} peak is attributed to stronger electron doping of MoS_2 on annealed HfO_2.

We have also examined the impact of dielectric screening in comparing MoS_2 on untreated HfO_2 and SiO_2. The dielectric environment plays a crucial role in influencing both the electronic bandgap and the exciton binding energy, which collectively determine the optical bandgap. When comparing HfO_2 to SiO_2, the enhanced screening effect in HfO_2 is expected to weaken electron−electron interactions, resulting in a reduction of quasiparticle bandgap renormalization.[25] Similarly, the electron−hole interactions are also reduced, leading to a decrease in the exciton binding energy. The overall shift in the PL depends on which of these two competing effects dominates. In our observations, the excitonic PL positions of MoS_2 on SiO_2 and HfO_2 show negligible differences, suggesting that the two effects may effectively cancel each other out—consistent with density functional theory (DFT) calculations.[26] Regarding defect-mediated PL, deep defect states arising from sulfur vacancies are positioned far from the band edges and are pinned below the conduction band edge with a fixed energy gap, as indicated by DFT calculations.[27] This configuration reduces the binding energy of excitons to the defect states, which is expected to enhance the delocalization of trapped excitons and lead to a decrease in defect-mediated PL intensity. However, our findings reveal an opposite trend in that the defect-mediated PL intensity increases in MoS_2 on HfO_2 compared to MoS_2 on SiO_2, indicating that other factors may be at play in this system.

To verify that the disappearance of the LX_D peak is related to substrate effects from SiO_2 and not the transfer process, we picked up defective MoS_2 from SiO_2 and transferred it onto another SiO_2 substrate that was separately annealed at 600 °C in Ar/H_2. The PL spectrum of defective MoS_2 shows a broad LX_D peak (Figure 2a, red curve), suggesting that annealing of SiO_2 is important in observing the LX_D peak in defective MoS_2. We prepared three samples per set to confirm our observations, as shown in SI, Figure S5. To compare the MoS_2 on untreated SiO_2 and on annealed SiO_2, we analyzed the PL spectra to extract the ratio of the integrated intensity of A^- trion to A exciton, $I(A^-)/I(A)$ (SI, Figure S6).[28] The $I(A^-)/I(A)$ ratio in defective MoS_2 on untreated SiO_2 (3.22) is higher than that on annealed SiO_2 (1.54), indicating that doping from annealed SiO_2 is suppressed. Similarly, pristine MoS_2 shows a higher $I(A^-)/I(A)$ ratio on untreated SiO_2 (0.44) than that on annealed SiO_2 (0.35). In pristine MoS_2 (Figure 2b), the $I(A^-)/I(A)$ ratio is much lower than in the defective MoS_2 samples, because the presence of sulfur vacancies introduces free electrons in the MoS_2.

We next analyze the effect of the HfO_2 substrate on LX_D PL emission from defective MoS_2 where we observe an opposite trend compared to that of MoS_2 on SiO_2. The LX_D peak can be observed when defective MoS_2 is transferred on untreated HfO_2. However, the LX_D peak disappears when the same defective flake is transferred onto a HfO_2 substrate that is preannealed in Ar/H_2 (600 °C, 30 min) (Figure 2c). A comparison of the Raman spectra of defective MoS_2 on both substrates shows that the A_{1g} mode is softened ($\Delta\omega = -0.6$ cm^{-1}) for annealed HfO_2, indicating that MoS_2 is more electron-doped by annealed HfO_2 than that by untreated HfO_2 (Figure 2d). The enhanced electron doping from annealed HfO_2 indicated by our results is similar to the doping from the annealed AlO_x substrate in a previous work.[29] These results

https://doi.org/10.1021/acs.jpcc.4c08491
J. Phys. Chem. C 2025, 129, 8294−8302

suggest that the annealing process to generate sulfur vacancies in MoS_2 also affects the surface states of the dielectric substrates, which determines the effective electron doping across the MoS_2/dielectric interface.

We have probed the change in dielectric surface states using WCA and XAS (SI, Figures S7 and S8). Briefly, we find that the WCA increases in annealed SiO_2 relative to untreated SiO_2—suggesting transformation of hydrophilic silanol (Si−OH) to hydrophobic siloxane (Si−O−Si) groups that suppress electron transfer to MoS_2 (SI, Figure S7).[30] This indicates that the origin of this electron doping from SiO_2 can be attributed to three possible mechanisms: (a) Lone-pair electrons on oxygen. The oxygen atom in a hydroxyl group has two lone pairs of electrons in the outer shell. These lone pairs are not involved in bonding and are relatively high in energy, making them available for donation. When MoS_2 is placed on a hydroxyl-terminated SiO_2 surface, the lone pairs on the oxygen atoms can interact with the conduction band of MoS_2, effectively donating electrons and causing n-type doping. (b) Surface dipole moment. Hydroxyl groups create a local dipole moment due to the electronegativity difference between oxygen and hydrogen. The oxygen atom has a partially negative charge, while the hydrogen atom has a partially positive charge. This dipole moment can induce an electric field at the interface between SiO_2 and MoS_2, facilitating electron transfer from the SiO_2 surface to the MoS_2 layer. (c) Surface states. Hydroxyl groups may introduce surface states within the bandgap of SiO_2. These states can act as electron donors if they are energetically aligned with the conduction band of MoS_2. Conversely, annealing the SiO_2 substrate at 600 °C in Ar/H_2 may remove these groups and lower the doping effect. In contrast, the WCA in HfO_2 decreases significantly after annealing. We attribute this behavior to the amorphous-to-polycrystalline phase transition in annealing HfO_2, as indicated by XAS spectra and X-ray diffraction patterns (SI, Figures S8 and S9).[31,32] The crystallization of HfO_2 at high temperatures is often accompanied by the generation of oxygen vacancies that could act as electron donors, altering the surface chemistry and leading to the observed changes in properties.[33]

Directly annealing monolayer MoS_2 on HfO_2 induces a similar suppression of the LX_D emission at RT (Figure S10). To confirm the suppression of LX_D emission on annealed HfO_2, the PL spectrum of MoS_2 on HfO_2 was measured as a function of temperature ranging from 300 to 10 K (Figure 3a). Even at 10 K, the A^-/A peak dominates over the B exciton peak (both are red-shifted by ∼55 meV) and no LX_D emission was observed. The PL spectra were also measured as a function of the excitation power (Figure 3b). The A^-/A peak remains the dominant peak for laser fluence ranging from 0.01 to 1.8 × 10^5 W cm^{-2}. The intensity of the A^-/A peak exhibits a linear dependence on excitation laser fluence ($I_{PL} \propto L_E^k$) with power exponent k = 0.96 (Figure 3c), suggesting that the A^-/A peak is excitonic emission that is typically associated with k = ∼1.[34]

To study the PL properties of MoS_2 without the influence of the substrate, we placed MoS_2 on hBN. hBN is atomically flat and has low density of charged impurities.[35] PL spectra of MoS_2 annealed on hBN (thickness ∼ 27 nm) at 10 K are shown in Figure 4. The optical microscopy image in Figure 4a shows that MoS_2 is partially located on HfO_2 and hBN. In Figure 4b, the PL intensity maps of the A^-/A peak and LX_D peaks measured at 10 K are shown, respectively. The A^-/A emission was observed in both MoS_2 on hBN and MoS_2 on

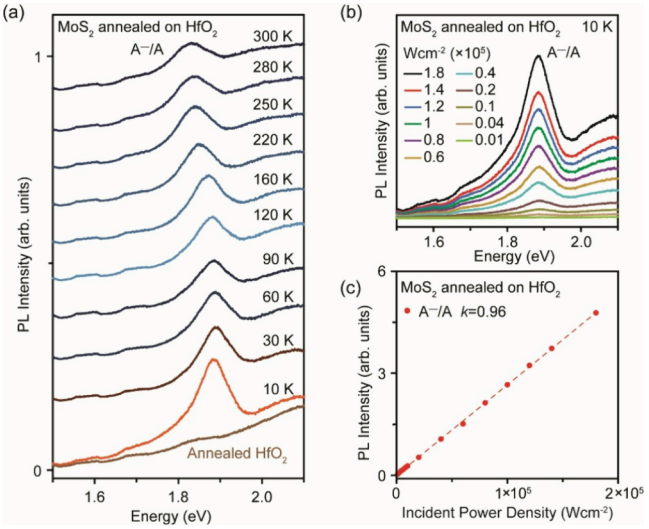

Figure 3. PL characterizations for MoS_2 annealed on HfO_2. (a) Temperature-dependent PL spectra measured at temperatures ranging from 300 to 10 K. (b) 10 K power-dependent PL spectra measured at laser fluence ranging from 0.01 to 1.8 × 10^5 W cm^{-2}. (c) Power-dependent PL intensity plot of the A^-/A peak measured at 10 K, showing linear dependence (power exponent k of 0.96) that corresponds to excitonic transition.

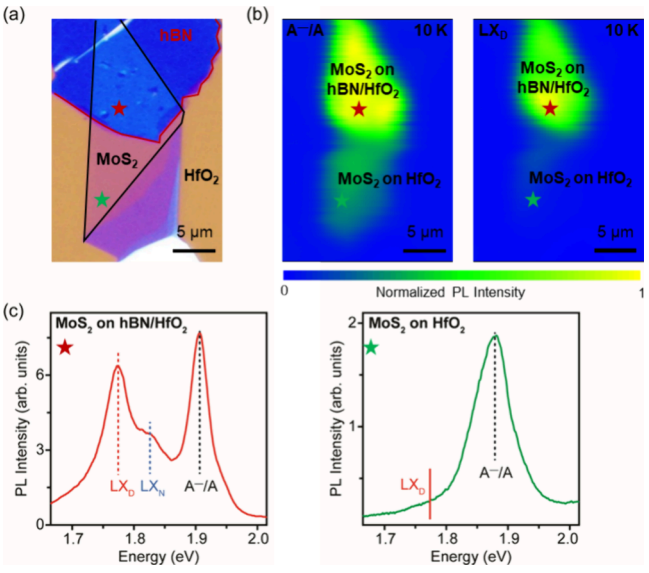

Figure 4. Intensity maps of A^-/A and LX_D emission in Ar/H_2 annealed (600 °C, 30 min) monolayer MoS_2 on hBN and MoS_2 on HfO_2. (a) Optical microscopy images of MoS_2 on hBN and MoS_2 on HfO_2. (b) Corresponding A^-/A and LX_D intensity maps measured at 10 K. A^-/A emission is distributed across MoS_2 on hBN and MoS_2 on HfO_2 [left panel in (b)], whereas LX_D emission is only observed in MoS_2 on hBN [right panel in (b)]. PL from two points is extracted from regions indicated by red and green stars in (a). (c) 10 K PL spectra, showing the LX_D peak in MoS_2 on hBN but not in MoS_2 on HfO_2.

HfO_2, whereas LX_D emission was only observed on MoS_2 on hBN. Furthermore, the spectrum from MoS_2 on hBN (indicated by the red star) and another spectrum from MoS_2 on HfO_2 (green star) were extracted. The LX_D peak is clearly visible for MoS_2 on the hBN region but is suppressed in MoS_2 on the HfO_2 region (Figure 4c). This result indicates that

https://doi.org/10.1021/acs.jpcc.4c08491
J. Phys. Chem. C 2025, 129, 8294−8302

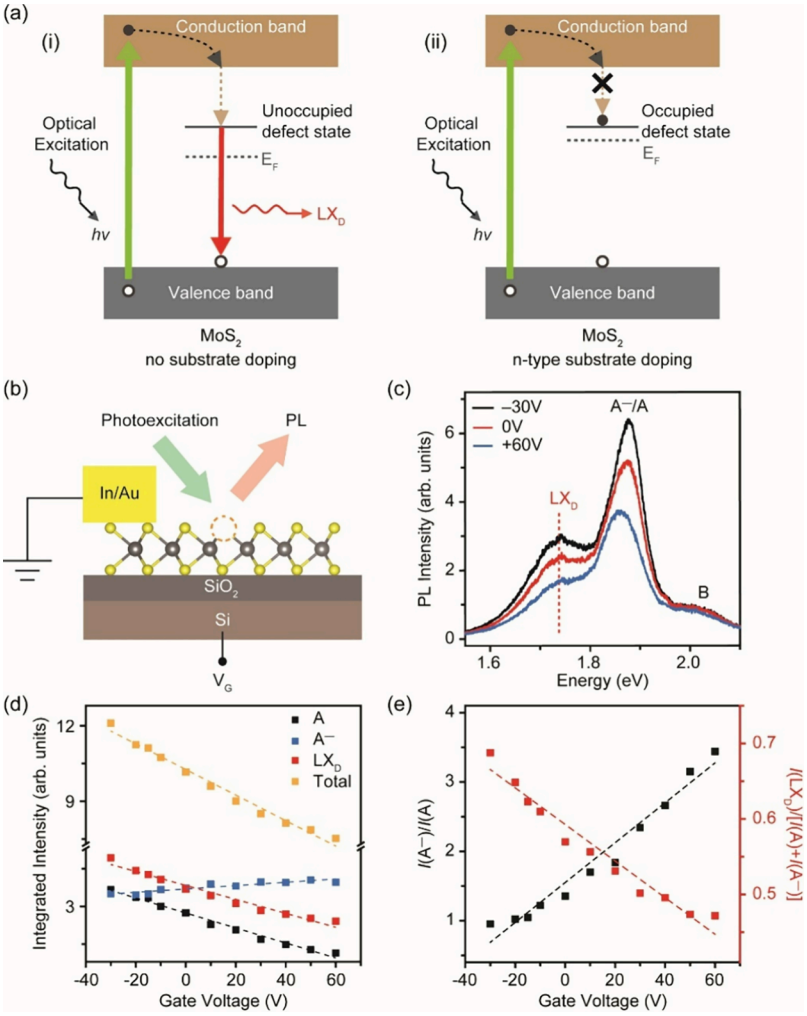

Figure 5. (a) Proposed schematic energy band diagram of defective monolayer MoS_2 with different doping levels. The horizontal dashed lines represent virtual Fermi levels, while the horizontal solid line represents real energy states due to defects. An electron is photoexcited from the valence band to the conduction band (denoted by the green arrow), relaxed to the conduction band edge (denoted by the black arrow), and then relaxed to the in-gap defect state (denoted by the yellow arrow). The localized electron at the defect state can be relaxed to the valence band edge and recombine with a hole, releasing a LX_D photon (denoted by the red arrow). The yellow arrow represents the trapping of excitons at in-gap states. For n-typed MoS_2 (ii), the Fermi level is higher with more valence electrons filling the in-gap states compared with undoped MoS_2 (i), thus suppressing the trapping of photoexcited electrons and reducing the defect-mediated radiative recombination. Gate dependence of the RT LX_D emission. (b) Schematic of MoS_2 FET and gate tuning of PL in defective monolayer MoS_2. (c) RT PL spectra of defective monolayer MoS_2 at different gate voltages (V_g). (d) Integrated intensity of A exciton, A^- trion, and LX_D peak, and their total contribution. (e) Relative intensity of trions, $I(A^-)/I(A)$, and the integrated RT PL intensity ratio of LX_D emission to the sum of A exciton and A^- trion emission, $I(LX_D)/[I(A) + I(A^-)]$, at different V_g. At negative V_g (hole doping), the LX_D emission becomes relatively stronger, while at positive V_g (electron doping), the LX_D emission becomes relatively weaker.

annealed hBN does not electronically dope MoS_2—even after annealing.

The above results indicate that the LX_D emission is suppressed in strongly electron-doped MoS_2. A simple energy band diagram of defective monolayer MoS_2 with different doping levels is shown in Figure 5a. In Figure 5a(i) for the undoped MoS_2 case, the Fermi level remains at midgap so that excited electrons can relax down to the unoccupied defect states of sulfur vacancies to form LX_D excitons, which can in turn radiatively recombine to emit the defect-mediated PL. In contrast, for the defective MoS_2, electron doping from substrate can occupy the sulfur vacancy states—shifting the Fermi level closer to the conduction band and the energy of the defect states (Figure 5a(ii)).[36] The occupation of the defect energy levels prevents relaxation of the excited electron to the defect state—preventing the formation of LX_D excitons and suppressing defect-mediated emission. While the preponderance of evidence suggests doping for suppression of the LX_D peak, other possibilities could also explain our observed results. For example, an alternative explanation for the disappearance of LX_D in electron-donating substrates (as-prepared SiO_2 and annealed HfO_2) is the short lifetime of free excitons due to rapid Auger recombination and/or the formation of free trions. That is, excitons annihilate before they have time to relax to the LX_D state. The occupation of the defect level may not be a necessary condition to prevent radiative recombination at LX_D because a defect-trapped electron can still, in principle, radiatively recombine with a hole in the valence band. We note that this model is developed based on the low laser fluence $\leq 17 \times 10^2$ W cm^{-2} under which the photodoping effect could be negligible. The effect of doping from the substrate is similar to electrostatic doping via

https://doi.org/10.1021/acs.jpcc.4c08491
J. Phys. Chem. C 2025, 129, 8294−8302

electrical gating—as previously reported by several groups.[28,37] To demonstrate the relevance of gate-modulated doping for defect-mediated PL emission, we fabricated field-effect transistors (FETs) using defective monolayer MoS_2 as the channel on 300 nm SiO_2/Si (see the schematic in Figure 5b). It can be seen that A^-/A decreases with increasing gate bias due to nonradiative recombination induced by the formation of trions, as observed previously by others.[38] Here, we also find that LX_D emission also decreases when the channel is n-doped due to filling of defect states (Figure 5c).[38] Deconvoluting the spectra reveals a monotonic decrease in the integrated intensities of the A exciton and LX_D peaks, whereas an increase in the A^- trion peak intensity is observed (Figure 5d). The $I(A^-)/I(A)$ ratio varied from 0.96 at $V_g = -30$ V (hole doping) to 3.44 at +60 V (electron doping).[28] The integrated PL intensity ratio of LX_D emission to the sum of A exciton and A^- trion emission, $I(LX_D)/[I(A)+I(A^-)]$, is inversely proportional to the $I(A^-)/I(A)$ ratio, confirming that electron doping reduces the defect-mediated emission LX_D (Figure 5e).

CONCLUSIONS

We have shown that sulfur-vacancy-mediated PL emission from MoS_2 depends on the electron doping level in MoS_2. At higher doping levels, the in-gap defect states induced by sulfur vacancies are occupied by electrons, which reduces the PL emission from localized excitons. The choice of a suitable dielectric substrate is therefore essential for observation of robust LX_D emission. Our results suggest that MoS_2 experiences more electron doping from the SiO_2 substrate as compared to HfO_2. The electron doping from the dielectric substrates originates from the presence of surface states that can be modified during the defect generation process. Our results provide useful considerations for building optoelectronic and sensing devices based on localized excitons in 2D TMDs.

EXPERIMENTAL METHODS

Sample Preparation. Monolayer MoS_2 was mechanically exfoliated from commercial bulk crystal purchased from 2D Semiconductor using a polydimethylsiloxane (PDMS)-assisted exfoliation method. Target MoS_2 flakes were dry-transferred onto target substrate (SiO_2 or HfO_2) and put in a 1 in. tube furnace. The samples were flowed with 450 sccm of N_2 (99.9999% purity) for 10 min to remove tube oxygen and then heated to 250 °C for 1 h under 100 sccm of N_2 to clean contaminants. hBN was directly mechanically exfoliated from commercial bulk crystal purchased from HQ Graphene onto target substrates.

Ar/H_2 Annealing of MoS_2. Samples were flowed with 450 sccm Ar/H_2 (95 vol %/5 vol %) for 10 min to remove tube oxygen and heated to 200 °C under 70 sccm Ar/H_2 for 10 min to remove tube moisture. Then, samples were heated to 600 °C and kept at that temperature for 30 min.

ALD Growth of HfO_2. The 50 nm HfO_2 films were grown on doped silicon substrates by using thermal ALD in a Veeco Fiji G2 reactor. A metal alkylamide hafnium precursor tetrakis (dimethyl amido)hafnium (TDMAH) was used as the Hf source, and deionized water was the oxygen source. The reaction has been reported as follows:[39] $Hf[(CH_3)_2N]_4 + 2H_2O \rightarrow HfO_2 + 4HN(CH_3)_2$. The TMDAH precursor was heated to 75 °C during the growth. The films were grown at a substrate temperature of 200 °C. At this temperature, the growth rate was estimated to be 1.2 Å/cycle. TDMAH and H_2O precursors were pulsed/purged per cycle for 0.25 s/10 s and 0.06 s/10 s, respectively. 60 sccm Ar was used as the carrier gas.

PC-Assisted Wet-Transfer Method. PC stamps were used to assist the transfer (SI, Figure S1). PC dissolved in chloroform was first drop-cast on the annealed sample to form a uniform film ①. A PDMS stamp was stacked on a glass slide and attached to the transfer stage with PDMS stamp face-down ②. The PDMS stamp was brought in contact with the PC stamp to form a firm stack ③. The PDMS/PC stack was raised to pick up the target flake from substrate 1 ④. The detached substrate 1 was replaced by another substrate 2 ⑤. The PDMS/PC stack was aligned and brought in contact with substrate 2 and heated to 180 °C for 1 min to melt PC and weaken the adhesion between PDMS and PC ⑥. The PDMS stamp was raised to detach from PC, depositing the target flake on substrate 2 ⑦. The sample was immersed in chloroform for 10 min to dissolve the melted PC stamp ⑧, leaving the target flake on substrate 2 ⑨.

Post Annealing of Transferred MoS_2 in Ar/H_2. Transferred samples were flowed with 450 sccm Ar/H_2 (95%:5%) for 10 min to remove tube oxygen and heated to 350 °C under 100 sccm Ar/H_2 and kept for 1 h to clean PC residues.

Measurement.

- Optical images of samples were taken on a Nikon Eclipsec LV150N optical microscope.
- RT Raman and steady-state PL spectra were collected on a Renishaw inVia confocal microscope using 532 nm laser excitation. Gate-dependent PL spectra were conducted at RT on a Horiba LabRAM 800HR confocal microscope connected to a Keithley 2400 source meter with 514 nm laser excitation. The incident fluence is kept below $\leq 17 \times 10^2$ W cm^{-2} to ensure minimal sample heating.
- Cryogenic PL spectra, PL mapping, and time-resolved PL measurements were measured on a Kymera spectrometer and Janis (ST-500) cryostat with a closed-cycle helium refrigerator. Continuous-wave 474 nm laser and pulsed 405 nm laser were used as excitations for PL spectra/mapping and time-resolved PL measurements, respectively. Long-pass filters and tunable bandpass filters were used to select the peaks during the time-resolved PL measurements.
- Contact angle was measured on FTA1000B dynamic contact angle analyzer.
- XAS measurements were performed at I06 beamline at Diamond Light Source, UK. The samples were measured at ~10^{-9} mbar. XPS measurements were performed at I09 beamline. The beam size was around 15 μm by 35 μm. The core level spectra of MoS_2 were acquired at photon energy of 1 keV. Samples were heated at 80 °C under 10^{-7} mbar for 1 h to remove physisorbed species prior to loading into a measurement chamber (10^{-10} mbar). The Fermi level was calibrated by using a clean Au foil in contact with the sample holder. The spectral resolution was determined by measuring and fitting the Fermi edge of a Au foil with a Gaussian broadened Fermi−Dirac distribution and was determined to be 0.21 eV.

https://doi.org/10.1021/acs.jpcc.4c08491
J. Phys. Chem. C 2025, 129, 8294−8302

- XRD was measured on a Bruker D8 Advance powder X-ray diffractometer using Cu Kα radiation, equipped with automatic divergence slits and a LynxEye-XE position sensitive detector.

■ ASSOCIATED CONTENT

Supporting Information

The Supporting Information is available free of charge at https://pubs.acs.org/doi/10.1021/acs.jpcc.4c08491.

Schematic of wet transfer of exfoliated TMDs across various substrates; optical images of exfoliated pristine MoS_2 before and after transfer from a SiO_2/Si substrate to another SiO_2/Si substrate; AFM images and PL spectra of transferred pristine monolayer MoS_2 and postannealed pristine monolayer MoS_2, respectively; synchrotron XPS spectra of the Mo 3d core level in pristine MoS_2 on untreated SiO_2 and on untreated HfO_2; deconvoluted RT PL spectra of transferred defective monolayer MoS_2 and pristine MoS_2 on untreated and annealed SiO_2, respectively; WCA measurement of (a) untreated/annealed SiO_2 and HfO_2; O *K*-edge XAS characterization of untreated/annealed SiO_2 and HfO_2; RT PL spectra of monolayer MoS_2 annealed on HfO_2; and XRD patterns of untreated and annealed HfO_2 (PDF)

■ AUTHOR INFORMATION

Corresponding Authors

Soumya Sarkar − *Department of Materials Science and Metallurgy, University of Cambridge, Cambridge CB3 0FS, U.K.*; orcid.org/0000-0002-9715-9004; Email: ss2806@cam.ac.uk

Manish Chhowalla − *Department of Materials Science and Metallurgy, University of Cambridge, Cambridge CB3 0FS, U.K.*; orcid.org/0000-0002-8183-4044; Email: mc209@cam.ac.uk

Authors

Yiru Zhu − *Department of Materials Science and Metallurgy, University of Cambridge, Cambridge CB3 0FS, U.K.*; orcid.org/0000-0002-1774-5311

Zhepeng Zhang − *Department of Physics, National University of Singapore, Singapore 117551, Singapore*

Ye Wang − *Department of Materials Science and Metallurgy, University of Cambridge, Cambridge CB3 0FS, U.K.*; orcid.org/0000-0003-1963-5105

Yang Li − *Department of Materials Science and Metallurgy, University of Cambridge, Cambridge CB3 0FS, U.K.*; orcid.org/0000-0003-2005-7381

Han Yan − *Department of Materials Science and Metallurgy, University of Cambridge, Cambridge CB3 0FS, U.K.*

Larissa Ishibe-Veiga − *Diamond Light Source, Didcot, Oxfordshire OX11 0DE, U.K.*

Anita Bagri − *Diamond Light Source, Didcot, Oxfordshire OX11 0DE, U.K.*

Ziwei Jeffrey Yang − *Department of Materials Science and Metallurgy, University of Cambridge, Cambridge CB3 0FS, U.K.*; orcid.org/0009-0002-0442-0080

Hugh Ramsden − *Department of Materials Science and Metallurgy, University of Cambridge, Cambridge CB3 0FS, U.K.*; orcid.org/0000-0002-0934-2088

Goki Eda − *Department of Physics, National University of Singapore, Singapore 117551, Singapore; Department of Chemistry, National University of Singapore, Singapore 117543, Singapore; Centre for Advanced 2D Materials, National University of Singapore, Singapore 117542, Singapore*; orcid.org/0000-0002-1575-8020

Robert L.Z. Hoye − *Inorganic Chemistry Laboratory, University of Oxford, Oxford OX1 3QR, U.K.*; orcid.org/0000-0002-7675-0065

Yan Wang − *Department of Materials Science and Metallurgy, University of Cambridge, Cambridge CB3 0FS, U.K.*; orcid.org/0000-0001-9241-3512

Complete contact information is available at: https://pubs.acs.org/10.1021/acs.jpcc.4c08491

Author Contributions

M.C. conceived the project. Y.Z. and S.S. designed the experiments under the supervision of M.C. Y.Z. prepared samples and performed RT steady-state PL/Raman spectroscopy measurement. S.S. and Y.Z. performed gate-dependent steady-state PL measurements. Y.L. and Ye.W fabricated FETs, and S.S. and Y.Z. performed gate-dependent PL measurements on the FETs. Y.Z and Ye.W. performed contact angle measurements and XAS measurements. L.I.-V. and A.B. assisted in the XAS measurements. Yan.W. and H.Y. fabricated In/Au electrodes and performed synchrotron XPS measurements. J.Y. performed XRD measurements. H.R. helped with the fitting of gate-dependent PL spectra. Z.Z. performed cryogenic steady-state PL measurements under the supervision of G.E. R.L.Z.H. helped with designing the experiments. All authors discussed the results and analysis. M.C., Y.Z., and S.S. wrote the manuscript, with input from all coauthors.

Notes

The authors declare no competing financial interest.

■ ACKNOWLEDGMENTS

We thank Prof. Sunmin Ryu of Pohang University of Science and Technology for discussions about the results. We acknowledge funding from European Research Council (ERC) Advanced Grant under the European Union's Horizon 2020 research and innovation program (grant agreement GA 101019828-2D-LOTTO]), EPSRC (EP/T026200/1, EP/T001038/1), and Grant supported by the Department of Science, Innovation and Technology and the Royal Academy of Engineering under the Chair in Emerging Technologies programme. We acknowledge Diamond Light Source for beam time on beamline I06 under Proposal MM36685 and beamline I09 under Proposal SI33391-1. R.L.Z.H. thanks the Royal Academy of Engineering through the Research Fellowships scheme (no. RF\201718\1701). G.E. acknowledges support from the Ministry of Education (MOE), Singapore, under AcRF Tier 3 (MOE2018-T3-1-005).

■ REFERENCES

(1) Bai, G.; Yuan, S.; Zhao, Y.; Yang, Z.; Choi, S. Y.; Chai, Y.; Yu, S. F.; Lau, S. P.; Hao, J. 2D Layered Materials of Rare-Earth Er-Doped MoS_2 with NIR-to-NIR Down- and Up-Conversion Photoluminescence. *Adv. Mater.* **2016**, *28* (34), 7472−7477.

(2) Zhang, Q.; Wee, A. T. S.; Liang, Q.; Zhao, X.; Liu, M. Defect Engineering of Two-Dimensional Transition-Metal Dichalcogenides: Applications, Challenges, and Opportunities. *ACS Nano* **2021**, *15* (2), 2165−2181.

(3) Yang, J.; Wang, Y.; Lagos, M. J.; Manichev, V.; Fullon, R.; Song, X.; Voiry, D.; Chakraborty, S.; Zhang, W.; Batson, P. E.; Feldman, L.; Gustafsson, T.; Chhowalla, M. Single Atomic Vacancy Catalysis. *ACS Nano* **2019**, *13* (9), 9958−9964.
(4) Li, L.; Qin, Z.; Ries, L.; Hong, S.; Michel, T.; Yang, J.; Salameh, C.; Bechelany, M.; Miele, P.; Kaplan, D.; Chhowalla, M.; Voiry, D. Role of Sulfur Vacancies and Undercoordinated Mo Regions in MoS_2 Nanosheets toward the Evolution of Hydrogen. *ACS Nano* **2019**, *13* (6), 6824−6834.
(5) Mitterreiter, E.; Schuler, B.; Micevic, A.; Hernangómez-Pérez, D.; Barthelmi, K.; Cochrane, K. A.; Kiemle, J.; Sigger, F.; Klein, J.; Wong, E.; Barnard, E. S.; Watanabe, K.; Taniguchi, T.; Lorke, M.; Jahnke, F.; Finley, J. J.; Schwartzberg, A. M.; Qiu, D. Y.; Refaely-Abramson, S.; Holleitner, A. W.; Weber-Bargioni, A.; Kastl, C. The Role of Chalcogen Vacancies for Atomic Defect Emission in MoS_2. *Nat. Commun.* **2021**, *12* (1), 3822.
(6) Zhang, Z.; Liang, H.; Loh, L.; Chen, Y.; Chen, Y.; Watanabe, K.; Taniguchi, T.; Quek, S. Y.; Bosman, M.; Bettiol, A. A.; Eda, G. Optically Active Chalcogen Vacancies in Monolayer Semiconductors. *Adv. Opt. Mater.* **2022**, *10* (23), No. 2201350.
(7) Koperski, M.; Nogajewski, K.; Arora, A.; Cherkez, V.; Mallet, P.; Veuillen, J. Y.; Marcus, J.; Kossacki, P.; Potemski, M. Single Photon Emitters in Exfoliated WSe_2 Structures. *Nat. Nanotechnol.* **2015**, *10* (6), 503−506.
(8) Parto, K.; Azzam, S. I.; Banerjee, K.; Moody, G. Defect and Strain Engineering of Monolayer WSe_2 Enables Site-Controlled Single-Photon Emission up to 150 K. *Nat. Commun.* **2021**, *12* (1), 3585.
(9) Li, Z.; Nameirakpam, H.; Berggren, E.; Noumbe, U.; Kimura, T.; Asakura, E.; Gray, V.; Thakur, D.; Edvinsson, T.; Lindblad, A.; Kohda, M.; Araujo, R. B.; Rao, A.; Kamalakar, M. V. Synchronized Photoluminescence and Electrical Mobility Enhancement in 2D WS_2 through Sequence-Specific Chemical Passivation. *J. Am. Chem. Soc.* **2024**, *146* (51), 35146−35154.
(10) Lin, Z.; Liu, W.; Tian, S.; Zhu, K.; Huang, Y.; Yang, Y. Thermal Expansion Coefficient of Few-Layer MoS_2 Studied by Temperature-Dependent Raman Spectroscopy. *Sci. Rep.* **2021**, *11* (1), 7037.
(11) Lloyd, D.; Liu, X.; Christopher, J. W.; Cantley, L.; Wadehra, A.; Kim, B. L.; Goldberg, B. B.; Swan, A. K.; Bunch, J. S. Band Gap Engineering with Ultralarge Biaxial Strains in Suspended Monolayer MoS_2. *Nano Lett.* **2016**, *16* (9), 5836−5841.
(12) McCreary, A.; Ghosh, R.; Amani, M.; Wang, J.; Duerloo, K.-A. N.; Sharma, A.; Jarvis, K.; Reed, E. J.; Dongare, A. M.; Banerjee, S. K.; Terrones, M.; Namburu, R. R.; Dubey, M. Effects of Uniaxial and Biaxial Strain on Few-Layered Terrace Structures of MoS_2 Grown by Vapor Transport. *ACS Nano* **2016**, *10* (3), 3186−3197.
(13) Ugeda, M. M.; Bradley, A. J.; Shi, S.-F.; da Jornada, F. H.; Zhang, Y.; Qiu, D. Y.; Ruan, W.; Mo, S.-K.; Hussain, Z.; Shen, Z.-X.; Wang, F.; Louie, S. G.; Crommie, M. F. Giant Bandgap Renormalization and Excitonic Effects in a Monolayer Transition Metal Dichalcogenide Semiconductor. *Nat. Mater.* **2014**, *13* (12), 1091−1095.
(14) Borghardt, S.; Tu, J.-S.; Winkler, F.; Schubert, J.; Zander, W.; Leosson, K.; Kardynał, B. E. Engineering of Optical and Electronic Band Gaps in Transition Metal Dichalcogenide Monolayers through External Dielectric Screening. *Phys. Rev. Mater.* **2017**, *1* (5), No. 054001.
(15) Raja, A.; Chaves, A.; Yu, J.; Arefe, G.; Hill, H. M.; Rigosi, A. F.; Berkelbach, T. C.; Nagler, P.; Schüller, C.; Korn, T.; Nuckolls, C.; Hone, J.; Brus, L. E.; Heinz, T. F.; Reichman, D. R.; Chernikov, A. Coulomb Engineering of the Bandgap and Excitons in Two-Dimensional Materials. *Nat. Commun.* **2017**, *8* (1), 15251.
(16) Ji, E.; Yang, K.; Shin, J.-C.; Kim, Y.; Park, J.-W.; Kim, J.; Lee, G.-H. Exciton-Dominant Photoluminescence of MoS_2 by a Functionalized Substrate. *Nanoscale* **2022**, *14* (38), 14106−14112.
(17) Nur, R.; Tsuchiya, T.; Toprasertpong, K.; Terabe, K.; Takagi, S.; Takenaka, M. High Responsivity in MoS_2 Phototransistors Based on Charge Trapping HfO_2 Dielectrics. *Commun. Mater.* **2020**, *1* (1), 103.
(18) Li, Y.; Steuer, O.; Lin, K.; Samad, F.; Sokolova, D.; Erbe, A.; Helm, M.; Zhou, S.; Prucnal, S. Influence of Dielectric Capping on the Optical Properties of Two-Dimensional Transition-Metal Dichalcogenides: Implications for Nano-Optoelectronics. *ACS Appl. Opt. Mater.* **2023**, *1* (10), 1733−1741.
(19) Tran, T. T.; Elbadawi, C.; Totonjian, D.; Lobo, C. J.; Grosso, G.; Moon, H.; Englund, D. R.; Ford, M. J.; Aharonovich, I.; Toth, M. Robust Multicolor Single Photon Emission from Point Defects in Hexagonal Boron Nitride. *ACS Nano* **2016**, *10* (8), 7331−7338.
(20) Munson, K. T.; Torsi, R.; Mathela, S.; Feidler, M. A.; Lin, Y. C.; Robinson, J. A.; Asbury, J. B. Influence of Substrate-Induced Charge Doping on Defect-Related Excitonic Emission in Monolayer MoS_2. *J. Phys. Chem. Lett.* **2024**, *15* (31), 7850−7856.
(21) Kim, G.; Kim, H. M.; Kumar, P.; Rahaman, M.; Stevens, C. E.; Jeon, J.; Jo, K.; Kim, K.-H.; Trainor, N.; Zhu, H.; Sohn, B.-H.; Stach, E. A.; Hendrickson, J. R.; Glavin, N. R.; Suh, J.; Redwing, J. M.; Jariwala, D. High-Density, Localized Quantum Emitters in Strained 2D Semiconductors. *ACS Nano* **2022**, *16* (6), 9651−9659.
(22) Zhu, Y.; Lim, J.; Zhang, Z.; Wang, Y.; Sarkar, S.; Ramsden, H.; Li, Y.; Yan, H.; Phuyal, D.; Gauriot, N.; Rao, A.; Hoye, R. L. Z.; Eda, G.; Chhowalla, M. Room-Temperature Photoluminescence Mediated by Sulfur Vacancies in 2D Molybdenum Disulfide. *ACS Nano* **2023**, *17* (14), 13545−13553.
(23) Sarkar, S.; Goswami, S.; Trushin, M.; Saha, S.; Panahandeh-Fard, M.; Prakash, S.; Tan, S. J. R.; Scott, M.; Loh, K. P.; Adam, S.; Mathew, S.; Venkatesan, T. Polaronic Trions at the $MoS_2/SrTiO_3$ Interface. *Adv. Mater.* **2019**, *31* (41), 1−9.
(24) Chakraborty, B.; Bera, A.; Muthu, D. V. S.; Bhowmick, S.; Waghmare, U. V.; Sood, A. K. Symmetry-Dependent Phonon Renormalization in Monolayer MoS_2 Transistor. *Phys. Rev. B* **2012**, *85* (16), No. 161403.
(25) Ryou, J.; Kim, Y.-S.; KC, S.; Cho, K. Monolayer MoS_2 Bandgap Modulation by Dielectric Environments and Tunable Bandgap Transistors. *Sci. Rep.* **2016**, *6* (1), 29184.
(26) Komsa, H. P.; Krasheninnikov, A. V. Effects of Confinement and Environment on the Electronic Structure and Exciton Binding Energy of MoS_2 from First Principles. *Phys. Rev. B: Condens. Matter Mater. Phys.* **2012**, *86* (24), No. 241201.
(27) Naik, M. H.; Jain, M. Substrate Screening Effects on the Quasiparticle Band Gap and Defect Charge Transition Levels in MoS_2. *Phys. Rev. Mater.* **2018**, *2* (8), No. 084002.
(28) Mak, K. F.; He, K.; Lee, C.; Lee, G. H.; Hone, J.; Heinz, T. F.; Shan, J. Tightly Bound Trions in Monolayer MoS_2. *Nat. Mater.* **2013**, *12* (3), 207−211.
(29) McClellan, C. J.; Yalon, E.; Smithe, K. K. H.; Suryavanshi, S. V.; Pop, E. High Current Density in Monolayer MoS_2 Doped by AlO_x. *ACS Nano* **2021**, *15* (1), 1587−1596.
(30) Park, K.; Kang, H.; Koo, S.; Lee, D.; Ryu, S. Redox-Governed Charge Doping Dictated by Interfacial Diffusion in Two-Dimensional Materials. *Nat. Commun.* **2019**, *10* (1), 4931.
(31) Khan, S. B.; Zhang, Z.; Lee, S. L. Annealing Influence on Optical Performance of HfO_2 Thin Films. *J. Alloys. Compd.* **2020**, *816*, No. 152552.
(32) Shim, J.; Rivera, J. A.; Bashir, R. Electron Beam Induced Local Crystallization of HfO_2 Nanopores for Biosensing Applications. *Nanoscale* **2013**, *5* (22), 10887−10893.
(33) Ni, J.; Zhou, Q.; Li, Z.; Zhang, Z. Oxygen Defect Induced Photoluminescence of HfO_2 Thin Films. *Appl. Phys. Lett.* **2008**, *93* (1), 11905.
(34) Tongay, S.; Suh, J.; Ataca, C.; Fan, W.; Luce, A.; Kang, J. S.; Liu, J.; Ko, C.; Raghunathanan, R.; Zhou, J.; Ogletree, F.; Li, J.; Grossman, J. C.; Wu, J. Defects Activated Photoluminescence in Two-Dimensional Semiconductors: Interplay between Bound, Charged, and Free Excitons. *Sci. Rep.* **2013**, *3*, 1−5.
(35) Buscema, M.; Steele, G. A.; van der Zant, H. S. J.; Castellanos-Gomez, A. The Effect of the Substrate on the Raman and Photoluminescence Emission of Single-Layer MoS_2. *Nano Res.* **2014**, *7* (4), 561−571.

https://doi.org/10.1021/acs.jpcc.4c08491
J. Phys. Chem. C 2025, 129, 8294−8302

(36) Hötger, A.; Klein, J.; Barthelmi, K.; Sigl, L.; Sigger, F.; Männer, W.; Gyger, S.; Florian, M.; Lorke, M.; Jahnke, F.; Taniguchi, T.; Watanabe, K.; Jöns, K. D.; Wurstbauer, U.; Kastl, C.; Müller, K.; Finley, J. J.; Holleitner, A. W. Gate-Switchable Arrays of Quantum Light Emitters in Contacted Monolayer MoS_2 Van Der Waals Heterodevices. *Nano Lett.* **2021**, *21* (2), 1040−1046.
(37) Ross, J. S.; Wu, S.; Yu, H.; Ghimire, N. J.; Jones, A. M.; Aivazian, G.; Yan, J.; Mandrus, D. G.; Xiao, D.; Yao, W.; Xu, X. Electrical Control of Neutral and Charged Excitons in A Monolayer Semiconductor. *Nat. Commun.* **2013**, *4* (1), 1−6.
(38) Lien, D.-H.; Uddin, S. Z.; Yeh, M.; Amani, M.; Kim, H.; Ager, J. W.; Yablonovitch, E.; Javey, A. Electrical Suppression of All Nonradiative Recombination Pathways in Monolayer Semiconductors. *Science* **2019**, *364* (6439), 468−471.
(39) Gieraltowska, S.; Wachnicki, L.; Dluzewski, P.; Witkowski, B. S.; Godlewski, M.; Guziewicz, E. Atomic Layer Deposition of HfO_2 Films Using TDMAH and Water or Ammonia Water. *Materials* **2023**, *16* (11), 4077.

https://doi.org/10.1021/acs.jpcc.4c08491
J. Phys. Chem. C 2025, 129, 8294−8302